IEEE Access
Multidisciplinary ⋮ Rapid Review ⋮ Open Access Journal

Received 24 February 2023, accepted 1 May 2023, date of publication 5 May 2023, date of current version 11 May 2023.

Digital Object Identifier 10.1109/ACCESS.2023.3273483

RESEARCH ARTICLE

Reverse Power Flow Due to Solar Photovoltaic in the Low Voltage Network

ISSAH B. MAJEED[1], (Member, IEEE), AND NNAMDI I. NWULU[2], (Senior Member, IEEE)
[1]Electrical and Electronic Department, University of Johannesburg, Auckland Park 2006, South Africa
[2]Center for Cyber-Physical Food, Energy and Water Systems, University of Johannesburg, Auckland Park 2006, South Africa

Corresponding author: Issah B. Majeed (issahmajeed@gmail.com)

ABSTRACT Distributed generation has enhanced power production in recent times. Due to their benefits, Ghana is interested in grid-tied solar photovoltaic (PV) systems. Despite the benefits, solar PV integration studies in Ghana have not advanced. This study examines reverse power flow (RPF) due to solar PV in Low Voltage (LV) network branches. The methodology uses a modified IEEE European test network and an Electricity Company of Ghana (ECG) LV network. ETAP software is used to simulate the two solar PV integrated LV networks, and the obtained data is used to formulate correlation models of solar PV penetration and key network parameters in Excel. Model results estimate the RPF critical values for the modified IEEE European test network and the ECG LV network as 7.36 kW and 7.44 kW, respectively. The RPF values are obtained at maximum penetration depths of 62.6% and 69.8% respectively. At maximum penetration levels, predicted line loadings are 6.42% and 7.28% respectively. Further analysis reveals branch-transformer RPF margins of 26.8% and 23.1% in the modified IEEE European test network and the ECG LV network respectively. The results are essential for establishing pre-determined settings to safeguard LV network branches and transformers from overload due to RPF.

INDEX TERMS Safe margins, low voltage network, reverse power flow, simulation data, solar PV, threshold parameters.

I. INTRODUCTION

In today's world, integrating PV systems into low and medium-voltage distribution networks is becoming increasingly frequent [1], [2], [3], [4]. It has been established in the literature that low-level penetration with grid-tied PV enhances the LV network through voltage improvement, system loss reduction, and transformer service life extension [5], [6]. The challenges associated with high-level penetration, on the other hand, include voltage rise and fluctuation, reverse power flow, exceeding transformer and cable ratings, increased power losses, and protective equipment issues [7], [8], [9].

With the potential rise in the adoption of solar PV technology, the current network infrastructure might not be able to handle high levels of penetration without proper regulations. Because LV networks are more likely to have random installations by customers, it is important to do impact assessment studies before accepting PV energy resources into the network [10]. However, it is possible to integrate a greater amount of PV generation into distribution networks while still maintaining operational and technical restrictions on the system, given that a more accurate high-impact assessment is done for PV generation in the networks [1].

One major objective of impact assessment investigations is the determination of penetration levels, which depends on the criteria for assessment. For instance, the depth of penetration of a distributed generator (DG) on a feeder is defined in several ways based on the impact factor [10], [11]. In [12] and [13], the depth of penetration is defined as the total PV nameplate rating to the annual circuit peak load on a feeder.

In particular, [14] observes that there is no benchmark for determining what constitutes a high penetration level for solar PV. Despite that, the works of [15] and [16] suggest that at penetration levels above 15% for peak feeder loads, the challenges of high PV penetrations become apparent. Another school of thought holds that the negative impacts are noticeable for penetrations between 20% to 30% of the

The associate editor coordinating the review of this manuscript and approving it for publication was Chandan Kumar.

total generation [17]. This makes it difficult to establish the maximum permitted penetration level which can be deployed on a feeder since it is dependent on a variety of factors, such as the electrical properties of the feeder, the location of PV systems, etc. [18]. Unfortunately, high penetration levels without network upgrades can negatively impact the network giving rise to reverse power flow.

According to [19], high PV penetration levels cause RPF, which is a phenomenon that develops when the amount of PV generation in a grid-tied network is more than the load demand. For this reason, the power flow from the grid may be reversed depending on the size and location of the installed solar PV system [20]. Thus, RPF can develop in various sections of the distribution network depending on the PV penetration depth. The distribution system is impacted in various ways by RPF under high PV injection levels. In [19], the authors used data from an 11 kV distribution feeder in South Australia to demonstrate that increasing PV penetration will increase the number of RPF events in a year, for a given load.

The study in [10] shows that RPF conditions can be related to various voltage rises and can cause a voltage rise as little as 1% above the nominal voltage anywhere on a feeder. Likewise, voltage control problems due to the impact of RPF resulting in voltage fluctuations and voltage rise in a distribution system have been reported in [21]. Publications [22], [23], [24], [25], [26], [27] also review the possibility of RPF increasing network load, overvoltage, and losses. In addition, unidirectional voltage regulators, are prone to failures when exposed to RPF. For this reason, the regulation of substation load tap changers could be impaired resulting in the incorrect operation of line drop compensators [8].

In related findings, protective mechanisms in distribution systems may have issues if the power flow is reversed. For instance, authors in [28] used an IEEE 13-nodes test feeder to demonstrate how the sensitivity of the protection coordination is affected by RPF. Similarly, relay miscoordination is reported in [29], where the authors used an IEEE 33 bus system to analyze the effects of RPF on the operation of protective devices in a distribution system. The outcome indicates that the protective mechanism is effective for PV penetration levels below 25%. For more than 25% PV penetration, however, increased reverse power flow, causes nuisance tripping and operating blindness.

Other protection issues are known to expose distribution system components to overloading. In particular, RPF is shown to coincide with an increase in voltage at the feeder terminals and frequently results in transmission line and transformer overloading [30]. Also, according to studies [31] and [32], the injection of a PV system into a feeder will gradually reduce the loading level. However, a further increase in the penetration reverses the power flow which ultimately overloads the feeder.

According to [33] overloading affects the line thermal limit which represents the current limit of each network branch. Therefore, an increase in feeder loading due to RPF may cause distribution feeders to reach their thermal limits. For instance, the violation of thermal limits in transmission lines can be due to reverse power flow resulting in the overloading of lines [30]. Authors in [31] have studied two Malaysian residential LV networks with high PV coverage. The network impact assessment methodology includes a Monte Carlo simulation. Results show that transformers and feeders in the two networks experience thermal limit violations due to high reverse power flow. Hence, in both networks, the feeders reach their thermal loading limit at about 80% PV penetration.

The thermal limitation of a line conductor is closely related to its static rating, or ampacity, which is its peak current-carrying capability. Static ratings are based on temperature and operational state assumptions that are fixed. These assumptions are based on the worst-case values anticipated for important environmental characteristics such as wind speed, ambient temperature, and sun radiation [34], [35]. For this reason, a given conductor can have several ampacities depending on its application and operational assumptions [36], [37].

It follows that, depending on system operating conditions, line thermal rating is related to the ampacity of the conductor; which restricts the penetration of solar PV in an LV network [13], [38]. The conductor ampacity restriction is used as an impact factor in [39] to investigate the maximum amount of solar PV that may be installed in a distribution system. The simulation was performed in Matlab®with the power flow program, MatPower. Results show that based on substation voltages in the range of 0.95 p.u and 1.05 p.u, line overload develops due to RPF caused by excessive PV penetration. The overload condition enabled the current to reach 221% of the conductor ampacity. Further results show that simulation data can be formulated and used to predict the amount of solar PV that can be installed without provoking line thermal overloads.

The thermal limit of a line is essential since the line protection system rating depends on it. This capability also allows for better management of the operation of power cables connecting the PV system to the grid [40]. Another management strategy proposed by [41] is the use of storage devices to reduce or eliminate the undesirable effects of RPF in a distribution network. The proposed strategy consists of a constant charging algorithm deployed on a real Australian three-phase distribution network. The results showed improvement in the three-phase voltages.

In [20], the authors present an impedance-based monitoring method for detecting PV penetration levels in a distribution network. The methodology is evaluated on the IEEE 34-node test feeder to demonstrate its effectiveness. A modified Maximum PowerPoint Tracker (MPPT) control algorithm is proposed in [42] to monitor and control reverse power flow in a low-load network. The methodology is evaluated using a grid-tied PV system coupled with a synchronous generator. Simulation results show that

the Multiple MPPT control switches limit RPF toward the generator.

In the current literature, distribution feeders are the main focus of investigation for assessing the impacts of high PV penetration [43], [44], [45], [46], [47]. Certain studies, however, investigate the impact of RPF due to high solar PV penetration in distribution feeders [48], [49], [50], [51]. For instance, the study in [52] illustrates the potential intensity of reverse power flows due to high penetration by scenario analysis on the main feeder. Other studies also focus on feeder protection schemes to limit reverse power flow [53], [54].

Moreover, fewer studies appear in the published literature on solar PV impact studies in Ghana [55], [56], [57], [58]. These studies are conducted as case or feasibility studies on 33 kV/16 kV sub-transmission networks with grid-tied or isolated LV feeders. It is observed that previous studies on RPF either scarcely or do not consider metrics that represent detailed network branch analysis. To address these gaps, the authors intend to broaden the scope of previous studies by focusing on metrics that account for the individual contributions of network branches exposed to RPF due to high solar PV impact. Therefore, the major motivation for this investigation is to provide utilities with the required framework for defining predetermined safe operation limitations for PV systems based on their impact on LV network branches. This will prevent the branches from line overload due to RPF resulting from high PV penetrations. The major goal of this research is to examine how the reverse power flow impacts branches in an LV network with high PV penetration.

The investigation networks for this study are a modified IEEE European test network and an ECG LV network in Ghana's western region. The networks are adopted to establish the effectiveness of the proposed methodology. The study will model and analyze the distribution networks using unconstrained simulation analysis in ETAP software. Thus, under high PV penetration, the branches will be investigated for overloads as RPF develops in the network. This will enable us to estimate the maximum allowable branch-based depth of PV penetration and quantify key network branch parameters.

The research will be conducted based on utility practices where PV deployment follows a systematic approach. The investigation is limited to a single-case scenario with continuous PV generation in an LV network with static loads. The study's findings suggest that network operators establish predetermined criteria to protect the network branches and substation transformers from overload due to RPF because of high PV penetrations. The following contributions fill the gaps that have been identified in the literature:

A statistical method is employed to develop correlation models for threshold analysis to predict:

1. Net reverse power flow and key network branch operating limits.
2. The branch-based maximum depth of solar PV penetration and branch-transformer RPF safe margin beyond which RPF will flow into the transformer.

The rest of this work is organized as follows: Methodology is discussed in detail in Section II. The two test networks are introduced and modeled in this section. Also, correlation models of solar PV and key branch network parameters are formulated from the simulation results. Section III is a discussion of the simulation and correlation model results. The summary results of the threshold analysis and branch-transformer margin are presented in this section. Finally, section IV draws conclusions and recommendations for future work.

A. GRID-TIED SOLAR PV POWER FLOW ANALYSIS

In this section, we examine the steady-state dynamics of the power flow between solar PV and the grid.

1) INVERTER-GRID POWER FLOW DYNAMICS WITH SOLAR PV INJECTION

Figure 1 illustrates the circuit model of a grid-connected single-phase solar module inverter. The grid is modeled as a voltage source, whereas the inverter is modeled as a current source with a high output impedance. A filter is required to reduce the ripples at the inverter output caused by harmonics [59]. The LCL filter system needs three passive elements: the inductor at the inverter output, L_1, the grid inductor, L_2, and the coupling capacitance, C, at the interphase. Assuming there are no losses to warrant damping resistors, the three state parameters are V_{inv}, V_{grid}, and V_C representing inverter, grid, and capacitor voltages respectively.

According to the model, there is an active power exchange between the inverter and the grid. The main aim of this circuit is to supply maximum active power to the grid.

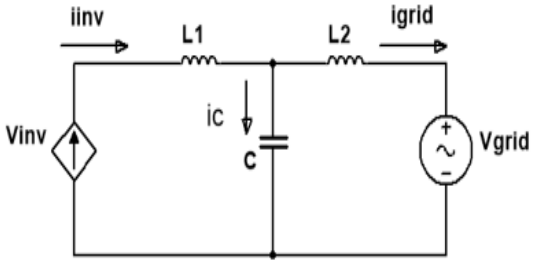

FIGURE 1. Equivalent inverter-grid interphase circuit.

A modification of [60] enables us to establish steady-state equations for the circuit in the continuous-time domain. Therefore, the following equations are obtained using the generalized Kirchhoff's laws:

$$\frac{\mathrm{di_{inv}}}{\mathrm{dt}} = \frac{V_{\mathrm{inv}} - V_{\mathrm{C}}}{L_1} \tag{1}$$

$$\frac{di_{\mathrm{grid}}}{dt} = \frac{V_{\mathrm{C}} - V_{\mathrm{grid}}}{L_2} \tag{2}$$

$$\frac{dV_{\mathrm{C}}}{dt} = \frac{i_{\mathrm{C}}}{C} = \frac{i_{\mathrm{inv}} - i_{\mathrm{grid}}}{C} \tag{3}$$

where,

$$i_{\text{inv}} = \text{inverter current}$$
$$i_{\text{grid}} = \text{grid current}$$
$$i_{\text{C}} = \text{capacitor current}$$

The state space transformation of (1) to (3) is realized with (4) in the frequency domain with Laplace transformation.

$$\begin{bmatrix} i_{\text{inv}^{(S)}} \\ i_{\text{grid}^{(S)}} \end{bmatrix} = \left(\frac{1}{s\,(L_1 + L_2)\,(s^2 \left(\frac{L_1 L_2 C}{L_1 + L_2}\right) + 1} \right) \times \begin{bmatrix} 1 + L_2 C s^2 & -1 \\ 1 & -\left(1 + L_2 C s^2\right) \end{bmatrix} \begin{bmatrix} v_{\text{inv}^{(S)}} \\ v_{\text{grid}^{(S)}} \end{bmatrix} \tag{4}$$

The most important reason for selecting the LCL filter is that it can be used at low switching frequencies [61]. Therefore, neglecting the high-frequency dynamics in (4),

$$s^2 L_1 C \approx 0 \; and \; s^2 L_2 C \approx 0$$

Equation (4) then reduces to the form in (5).

$$i_{\text{inv}}(s) \approx i_{\text{grid}}(s) \approx \frac{1}{s\,(L_1 + L_2)} \cdot (V_{\text{inv}}(s) - V_{\text{grid}}(s)) \tag{5}$$

The following condition must be met at the connection point for active power transfer:

$$|V_{\text{inv}}(t)| = \left|V_{\text{grid}}(t)\right| \tag{6}$$

The inverter is operated in a constant power factor mode with a unity power factor setting [62]. This is necessary for maximum power output into the grid. Hence it can be shown from (5) and (6) that the injected active power, P_{active} into the grid at a load point is given by (7):

$$P_{\text{active}} = \frac{|V_{\text{inv}}|\,\left|V_{\text{grid}}\right|}{\omega(L_1 + L_2)} \tag{7}$$

2) LOAD-POINT POWER FLOW DYNAMICS WITH SOLAR PV INJECTION

The solar PV system supplements the grid in significant ways by solar generation into the grid at a designed location. However, the injection of solar PV at a load point should not cause RPF, which can create overload conditions on the adjacent line feeding the load point from the grid. The steady-state dynamic expressions for the active power flow at an injection point and the line overload condition are given in (8) and (9) respectively.

$$P_{\text{b}}^{\text{line}}(t) = P_{\text{i}}^{\text{load}}(t) - P_{\text{i}}^{\text{pv}}(t) \forall t \tag{8}$$
$$I_{b\max,t} > \left|I_{\text{b,t}}\right| \forall t, \forall b \in \text{BRANCH} \tag{9}$$

$P_{\text{b}}^{\text{line}}(t)$ and $P_{\text{i}}^{\text{load}}(t)$ are time-specified active powers on the b_{th} branch and i_{th} load point respectively. The active power injected by the solar PV at the i_{th} load point in a specific period is $P_{\text{i}}^{\text{pv}}(t)$. Given that the LV lines have static ratings, then $I_{\text{bmax,t}}$, the maximum current rating or the ampacity of the b_{th} branch at a given time, always remains the same. This assumption makes (9) valid for all branches in the LV network for balanced three-phase loads. However, thermal capacity can be reached in one of the phases considering unbalanced three-phase loads [63]. Here, $\left|I_{b,t}\right|$ denotes the absolute value of the current in the b_{th} branch in a specific period. Therefore, we define the percentage line loading as follows:

$$\%\ \text{line loading} = \frac{\left|I_{\text{b,t}}\right|}{I_{\text{bmax,t}}} \times 100 \tag{10}$$

RPF appears to be localized in different network zones, indicating that its development is not concurrent [46]. This shows that RPF events occur at different periods in different locations within the grid. The situation becomes more complex with dispersed solar PV generation. However, these individual RPF contributions result in a net power flow, which is what is seen by the substation transformer with excess PV injection. Therefore, by neglecting power losses on network components and inverters, the grid net active power flow can be defined as the sum of the individual branch's active powers. When (8) is applied to successive load points, it is observed that the currents in the branches interact and add up or cancel out. The net APF (Active power flow) in the branches at each penetration level is then defined by the expression in (11):

$$P_{\text{net}}^{\text{line}}(t) = \sum_{t=1}^{N} \sum_{b=1}^{M} P_{\text{b}}^{\text{line}}(t) \quad \forall t \tag{11}$$

where $P_{\text{net}}^{\text{line}}(t)$ is the net active line power in a specific period, N is the total period for solar PV injection, and M is the total number of branches in the network. During normal operating conditions, active power flows from the grid to the various loads connected to the load points.

The variation of the magnitude of the aggregated active power of the solar PV injected and net active power consumed in the network at a given period creates the conditions for RPF. Three conditions define the RPF modes when the network branches are subjected to increased solar PV penetration through a load point. Combining (8) and (10), these conditions are explained by the relation in (12) [51].

$$P_{\text{net}}^{\text{line}}(t) = \begin{cases} \text{noRPF}; \sum_{i=1}^{N} P_i^{\text{load}}(t) > \sum_{i=1}^{M} P_{\text{i}}^{\text{pv}}(t) \forall t \\ \text{ThresholdofRPF}; \sum_{\text{i}=1}^{N} P_{\text{i}}^{\text{load}}(t) = \sum_{\text{i}=1}^{M} P_{\text{i}}^{\text{pv}}(t) \forall t \\ \text{RPF}; \sum_{\text{i}=1}^{N} P_{\text{i}}^{\text{load}}(t) < \sum_{\text{i}=1}^{M} P_{\text{i}}^{pv}(t) \forall t \end{cases} \tag{12}$$

Notably, due to excessive solar injection, RPF developing in isolated branches may not necessarily lead to power flow toward the substation transformer. On the other hand, RPF may also develop in isolated branches when a sudden drop in load occurs [42]. In both cases, the development of RPF at a load point may not have any significant effect on neighbouring branches. However, when RPF is sustained, the total RPF branches in the network can reverse the substation's conventional flow of power.

In [10], [14], and [64] the authors considered various definitions of PV depth of penetration depending on network

limiting factors. In this study, the operational definition of the depth of penetration, DP is obtained with respect to the active power in the LV network branches, expressed in (13):

$$\mathrm{DP} = \frac{\sum_{i=1}^{N} P_i^{pv}(t)}{\max(\sum_{b=1}^{M} P_b^{line}(t))} \times 100\% \tag{13}$$

In a related form, (14) shows that the network branch-based depth of penetration, D_B is a function of the net branch's active power, $P_{net}^{B}(t)$ in a specific period. Therefore, the solar PV depth of penetration can be described as follows:

$$D_{\mathrm{B}} = f(P_{\mathrm{net}}^{\mathrm{B}}(\mathrm{t}) > 0) \quad \forall \mathrm{t} \tag{14}$$

Equation (14) indicates that even though, the active power supplied to the branches by the solar PV may result in isolated cases of RPF, the net branch APF is not exceeded by the power injection from the solar PV. Further PV generation will result in an increased number of RPF events in the branches until a maximum depth of penetration, D_{Bmax} is attained. Therefore,

$$D_{\mathrm{Bmax}} = \lim_{p_{\mathrm{net}}^{B}(t)\to 0} D_{\mathrm{B}} \quad \forall t \tag{15}$$

According to (15), the branch-based maximum PV penetration occurs at the RPF margin when the net APF in the branches gradually decreases to zero. This study will establish that beyond the maximum penetration level, a safe margin must be exceeded to sufficiently reverse the power flow into the substation transformer.

3) ESTABLISHMENT OF BRANCH-TRANSFORMER RPF MARGINS

The branch-transformer RPF analysis establishes a relationship between the branch and transformer-based maximum penetration depths. Figure 2 depicts the profile of the RPF as it progresses in the network branches toward the substation transformer.

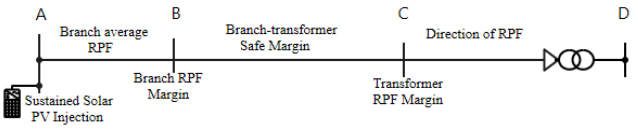

FIGURE 2. RPF operating profile in an LV network.

The profile makes it possible to determine the branch-transformer margin in the RPF mode. At the initial stage of sustained PV injection at A, a few network branches experience RPF. Continuous PV injection increases the number of individual branches with RPF as the net APF in the branches gradually diminishes to zero. At the branch RPF margin, B, the net branch APF eventually reaches zero. The transition from B to C represents the branch-transformer safe margin. Point C represents the transformer RPF margin beyond which RPF reaches the substation transformer. CD represents a period when reverse power flows into the transformer.

TABLE 1. Summary of RPF impact profile in an LV network.

RPF profile	RPF progression	Significance
A	• Net branch APF is zero. RPF flows.	
AB	• Branch average RPF increases.	• Presence of isolated RPF in branches
B	• Significant RPF in branches	• Potential overloading of lines beyond this point. • Determination of max. depth of penetration
BC	• Branch-transformer safe margin	• Overloading of lines may occur
C	• Transformer operating APF is zero. • Margin of RPF at the transformer	• Determination of max. depth of penetration
CD	• RPF progresses into the transformer	• Transformer overload and overheating of windings. • Excessive tripping

Beyond D, RPF may progress toward the medium-voltage (MV) network [65].

Table 1 provides an overview of the RPF progression from the branches toward the transformer. It details the significance of each point and the transitions between the points shown in Figure 2. For instance, the significance of point B is that there is potential overloading of lines beyond this point. Also, the branch-based maximum depth of PV penetration can be determined at point B (15).

A similar argument is used to establish the transformer-based maximum depth of penetration with RPF as an impact factor at point C. Consider a constant active power flow at a load point with solar PV injection. The transformer's operating APF, $P_{\mathrm{TX}}(\mathrm{t})$ decreases to zero with increased PV penetration. Beyond the critical point $P_{TX}(t) = 0$, RPF flows into the transformer. It follows that the transformer-based APF is related to the depth of penetration. Therefore,

$$D_{\mathrm{Tx}} = f(P_{\mathrm{Tx}}(\mathrm{t})) > 0 \forall \mathrm{t} \tag{16}$$

Hence, from (16), the transformer-based maximum depth of penetration, D_{Txmax} can be deduced as follows:

$$D_{\mathrm{Txmax}} = \lim_{p_{Tx}(t)\to 0} D_{\mathrm{Tx}} \quad \forall \mathrm{t} \tag{17}$$

Using (15) and (17), we can establish the following relation for the branch-transformer RPF Margin.

$$\text{Branch-Transformer RPF Margin} = (\mathrm{D_{Tx\ max}} - \mathrm{D_{B\ max}}) \tag{18}$$

The branch-transformer RPF margin expressed in (18) is observed as an excess kVA or percentage solar PV injection as RPF progresses. It is the region between the period when the net APF in the branches, starting from zero, assumes negative values to the critical point when the transformer operating active power is zero. This region is considered safe for the substation transformer since no violation of the conventional

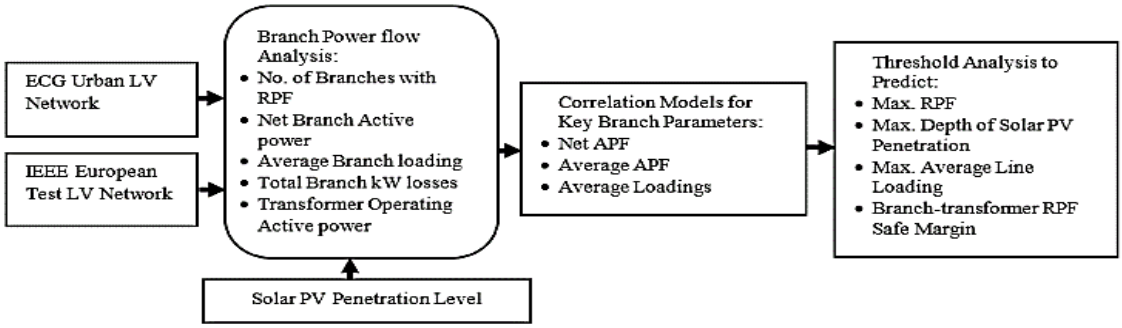

FIGURE 3. Design scheme for reverse power flow assessment on LV network branches.

flow of current is observed. However, beyond this region, the transformer may exceed its overload limits leading to excessive tripping and disconnection [66].

II. METHODOLOGY

This research assesses the development of RPF and overload conditions in the LV network branches caused by high PV penetration. The assessment is based on designed simulations on two networks, a modified IEEE European test network, and an ECG LV network. The method used required modeling and simulation of the networks using ETAP software's power flow calculation tool [67], [68].

The approach involves the deployment of solar PV units to each of the networks cumulatively at different penetration levels, based on a dispersion rule, and constraints such as voltage limit and the thermal limit which are enforced in the simulations. The PV allocation is based on a utility's system planning concept, unlike a customer-based installation where solar PV allocation is randomized [10]. The power flow calculations in ETAP software use unconstrained simulation on the LV networks. Based on the simulation data, correlation models are formulated for PV penetration depth and key network parameters such as APF, line loadings, and kW losses. The models predict violations in the line loadings, and the RPF and estimate the maximum penetration depth of solar PV in the network. Furthermore, the region beyond which RPF flows into the substation transformer is established.

A. IMPACT ANALYSIS FRAMEWORK

The design process for the proposed impact-assessment model for the study is presented in Figure 3. The assessment is based on the quantification of the impact of PV penetration in the evolution of RPF on LV network branches. Using simulations, two LV networks are considered to demonstrate the methodology: a modified IEEE European test network and a typical ECG distribution network.

Based on the power flow analysis, branch, and transformer operating parameters are examined under high-impact PV penetration. The simulation results are formulated as correlation models to quantify the impact of PV penetration on key network parameters such as APF, line loading, and kW losses. Furthermore, the models predict the maximum allowable penetration depth of solar PV, and violations in the line loadings and estimate the RPF in the branches of the LV network.

B. CASE STUDY NETWORKS

The configurations of the two test networks used to explain the methodology are given in the following sections.

1) A MODIFIED IEEE EUROPEAN TEST NETWORK

The low voltage test feeder is a 50 Hz radial distribution feeder. At the substation, a transformer connects the feeder to the medium voltage (MV) system. The transformer rating is 800 kVA, 11/0.416 kV Delta-Y, three-phase connection. The main feeder and laterals are at the voltage level of 416 V phase to phase. A detailed description of the network is found in [69]. In this network transformer, the full load rating is 128.8 kVA. This rating determines the level of PV injection into the network. The one-line diagram of the test feeder is shown in Figure 4:

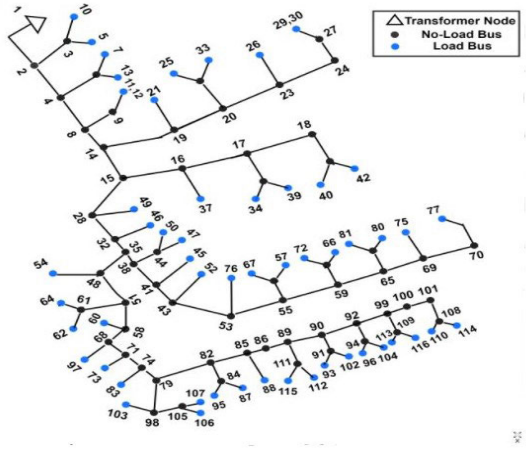

FIGURE 4. A Modified test case of IEEE European LV network [69].

2) ECG LV NETWORK

An LV network in a residential area of Sekondi-Takoradi Metropolis of Ghana is used as a case study grid in this study.

This network is connected to the MV grid by a Delta-Y pole-mounted transformer rated at 315 kVA, 11/0.415 kV. The LV lines are the secondary feeder lines with a size 50 mm^2 aluminium bare conductor. The allowed ampacities for the branches and cables used for the line loading evaluations are 249 A and 500 A, respectively. Single-phase multiple laterals, mostly make up the network.

This network features poor bus voltages at load locations, mainly caused by an increase in demand from customers or insufficient capacity in the network to meet the growing load. The single-line diagram of the ECG LV Network is depicted in Figure 5.

Standard procedures for improving voltages in the network include zoning, stringing additional lines to customer locations, or new transformer injection. One potential solution to improve voltage inadequacy is to install solar PV units at load locations with low voltages. By generating solar power at or near the load, the amount of power being drawn from the grid can be reduced, resulting in bus voltage improvement. This approach is used on the network to test the viability of the mitigation under high-impact solar PV.

Initially, the peak load rating for the transformer is determined and used to compute the PV penetration levels. The peak current obtained from the load monitoring on the ECG's C96 distribution transformer is 223 A. It follows that:

$$\text{Total kVA} = \frac{\sqrt{3}I_l V_l}{1000} = \frac{\sqrt{3} \times 223 \times 415}{1000}$$

Therefore, the full-load rating of the transformer is 160.29 kVA.

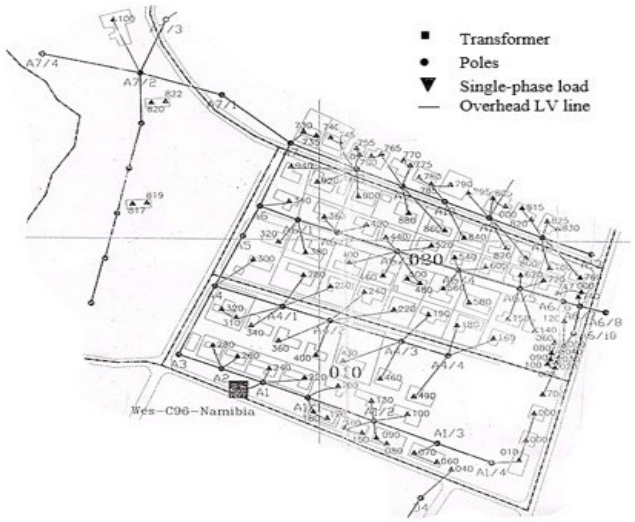

FIGURE 5. A Test case ECG LV network.

C. MODELING AND SIMULATION OF SOLAR PV INTEGRATED LV NETWORK

The two test networks were modeled with field data in the ETAP software. In each case, solar PV units were dispersed in the network according to the approach outlined previously.

1) MODELING OF DISTRIBUTION SYSTEM COMPONENTS

The two distribution networks are modeled and simulations are carried out on each network by load flow calculations in ETAP software.

The equipment editor was used to model the main LV network components.

2) THE SOURCE FEEDER

The source equipment is represented by an 11 kV three-phase power grid as the swing. In a typical case of the ECG network, a substation transformer steps down an 11 kV feeder source into a 0.415 kV operating voltage source. The distribution feeder, with service branches, is run throughout the network from this source. The values of these parameters for the grid in both networks are presented in Table 2.

3) NETWORK LOADS

These are customer loads modeled at load points as lumped static loads. These household loads were modeled as constant impedance three-phase loads. Loads on service poles were shared unequally across the phases to reflect standard practices. Typical average rated loads of 3.85 kVA and 1.90 kVA were used for the ECG LV network and the modified IEEE European test network respectively. Table 3 presents the data required for modeling the loads in both networks.

TABLE 2. Source data for the primary substation.

11 kV Feeder source parameter	Value	
Test Case	ECG Network	Modified IEEE European Network
Nominal voltage	11.5 kV	11.5 kV
Operating voltage	11 kV	11 kV
Base Power	100 MVA	100 MVA
Short circuit Rating	31.8 MVA (three-phase)	57.16 MVA (three-phase)
Source Configuration	Wye	Wye

TABLE 3. Typical household load data used for modeling static load.

Load parameter	Value	
Test case	ECG network	Modified IEEE European network
Section Id	Lump 59	Load 2
Load type	Constant kVA=80% constant Z=20%	Constant kVA=80% constant Z=20%
Nominal Voltage	240 V/415 V	240 V/416 V
Typical Connected load	2.75 kVA	1.90 kVA
Configuration	Delta	Wye
Power factor	0.85	0.85
Customer type	Residential	Residential
Load factor	0.9	0.9
Load distribution	lumped load, unbalanced	lumped load, balance

4) SUBSTATION TRANSFORMER

The transformer was modeled as a two-winding transformer to accommodate the network's maximum system loads. In the IEEE European network, the two-winding transformer was modeled as 11 kV/0.416 kV with an 800 kVA rating. Table 4 shows additional modeling parameters for both networks.

TABLE 4. Two-windings distribution transformer data.

Parameter	Value	
Test case	**ECG Network**	**Modified IEEE European network**
Section Id	C96	TR1
Frequency	50 Hz	50 Hz
Type	Three-phase core	Three-phase core
Nominal Rating	315 kVA	800 kVA
Primary Voltage	11 kV L-L	11 Kv L-L
Secondary Voltage	0.415 kV L-L	0.416 kV L-L
Sequence Impedance	$Z_0 = 4\%$, $Z_1 = 4\%$, $X_0/R_0 = 1.5\%$, $X_1/R_1 = 1.5\%$	$Z_0 = 4\%$, $Z_1 = 4.02\%$, $X_0/R_0 = 10\%$, $X_1/R_1 = 10\%$
Configuration	Primary, delta Secondary, wye	Primary, delta Secondary, wye
Phase Shift	Dyn11	Dyn11
Insulation Type	Liquid-filled	Liquid-filled

5) OVERHEAD LINES

The three-phase overhead lines were modeled as single lines, to represent feeder lines linking the load points. These lines span an average of 50 m between load points. A typical line conductor is an ACSR (aluminium conductor steel reinforced) with an ampacity of 249 A and operates at a maximum temperature of 75 degrees Celsius. Other modeling parameters are shown in Table 5. The convergence criteria for the simulation are shown in Table 6.

TABLE 5. Overhead line parameters at constant static ratings.

Parameter	Value	
Test case	**ECG network**	**Modified IEEE European network**
Equivalent Impedance	Positive sequence Zero sequence, 21 ohms	Positive sequence Zero sequence, 21 ohms
Conductor Type	LV, 50 mm^2 ACSR	LV, 49.5 mm^2 ACSR
Maximum Span	LV, 50 m	LV, 20 m-50 m
Nominal Ampacity	LV, 249 A	LV, 249 A
Maximum Temperature	75^0C	75^0C

6) MODIFIED IEEE EUROPEAN TEST NETWORK

The LV network was modeled to emulate a weak network with three-phase balanced loads in ETAP software. This test system includes a two-winding transformer of 0.8 MVA, 117 buses, and 55 loads. The following modifications were made in the modeling process:

TABLE 6. Convergence criteria for power flow simulation.

Factor	Operation
Computation Method	Adaptive Newton-Raphson
Convergence Parameters	0.0001 tolerance
	99 iterations
Computation Options	Assume line transposition
	Include line charging

- All single-phase loads were changed into 3-phase lumped loads
- Rating of loads: 0.69-3.8 kVA; total rated loads: 0.116 MW
- The bus coordinates in the original data were not considered.

7) ECG LV NETWORK

The ECG LV network was modeled using the ETAP software with a total of 78 poles representing the load points. Individual loads were connected to the load points as lumped three-phase loads, totaling 158.95 kVA.

Using the convergence criteria described in Table 6, we run a load flow simulation to evaluate each network's steady-state operating conditions due to the impact of cumulative PV penetration. The simulations were based on imposed restrictions, such as voltage and thermal constraints, to ensure network integrity as proposed by [70]. In this study, network restrictions for the assessment of bus voltage and branch loading (current) to prevent overload must satisfy the conditions presented in (19) and (20):

$$\text{load bus voltage} : 1.05\text{p.u} \geq v_{\text{load point}} \geq 0.95\text{p.u} \quad (19)$$

$$|I_{\text{branch}}| \leq 100\% \text{ of rated value} \quad (20)$$

In (19), $v_{\text{load point}}$ is the nominal voltage at the load point connected to the network. A load-point or a branch in the network most affected by the PV penetration is identified as a hotspot given that: (a) an over-voltage or under-voltage at a load point exceeds ±5% of a nominal voltage (19), or (b) a steady- state power flow that exceeds the thermal rating of a branch conductor according to (20). The thermal rating condition also applies to unbalanced three-phase loads such as the case in the ECG network (Table 3).

The simulation results obtained in the two networks were used to create mathematical models using the least square method [71]. The models involved relationships between solar PV penetration depth and key network parameters such as APF, line loadings, and kW losses. The statistical models obtained predict the RPF and estimate the maximum penetration depth of solar PV in each of the networks. These outlined approaches were also applied to the modified IEEE European test network.

8) SOLAR PV SELECTION AND DEPLOYMENT CRITERIA

The solar PV plant was modeled at a maximum power of 21.69 kW and a DC bus voltage of 1000V (Vdc). A three-phase inverter unit with an AC rating of 0.415 kV and 19.93 kVA forms part of the PV system. Based on the load demand in the network, the inverter was designed for continuous output power. The photowatt solar plant for large-scale grid-tied systems in the ETAP database met the specifications of the LV networks.

TABLE 7. ETAP solar PV modeling parameters.

PV Panel	
Manufacturer	Photowatt
Model	PW6-110
Type	Multi-crystalline
Size	110
Number of cells	36
Maximum Vdc	1000
Power factor	1
Watt/Panel	110.3
Number in series	20
Number in Parallel	10
Irradiance/ W/m2	1000
Ta/degree Celsius	30
Tc/ degree Celsius	5
MPP kW	21.69
Amps, dc	64.2

TABLE 8. ETAP data for solar PV three-phase inverter.

DC rating	
kW	22.06
V	343.6
FLA	64.2
%Efficiency	90.34
AC rating	
kVA	19.93
kV	0.415
FLA	27.73
%PF	100
Imax	150%

In this study, the inverter was designed without considering harmonics. Tables 7 and 8 present the data for the solar PV design.

In the literature, various methods are used to deploy solar PV units in distribution networks based on network constraints [17], [18], [72], [73]. In [68], for instance, the authors examine the effect of high PV penetrations on steady-state performance and transient stability using the IEEE 9-bus test system. Their findings indicate that high penetrations at distinct bus locations along the same feeder result in varied maximum penetration levels. In certain studies, scenarios are generated randomly for each PV penetration [19], [74]. For instance, customers may install solar PV at random locations that do not conform to the utility's design plans [1]. The utility-based allocation, however, is well defined to fit into their system planning strategies. This study adopts a modification of the utility-based approach.

In the present study, PV penetration was achieved by distributing PVs one at a time on the base-case model network. PV s were allocated to the worst load point with a voltage below 0.95 p.u. After each phase of PV injection, load flow calculations were performed. The PV placement procedure was then repeated until sufficient RPF was developed in the network for the transformer loading (kW) to register negative values. Steady-state power flows in network branches, load-point voltages, transformer details, and system losses were observed. The following pseudocode describes how solar PVs were distributed at the load points on each of the modeled LV networks:

Pseudocode for Solar PV dispersion

1. Start;
2. Perform a power flow analysis in the absence of a solar PV unit in the LV network;
3. Locate and position a solar PV unit at the lowest voltage bus, below 0.95 p.u;
4. Perform a power flow analysis for the LV network;
5. Identify branches with RPF and observe transformer operating loading (kW);
6. Repeat steps 3 to 5 until transformer operating loading (kW) registers negative values;
7. End.

9) DETERMINATION OF BRANCH-TRANSFORMER MARGIN

The theoretical concept of the branch-transformer margin is detailed in the previous section. This region is determined on the scale of minimum values of the branch and transformer active power as PV injection is sustained in the network. These conditions determine the transformer and branch-based maximum penetration depth at the RPF margins (see Figure 2). The RPF margin parameters were obtained from the simulation data generated from the two networks. The method of determining the branch-transformer margins applied to the two test networks is based on the following pseudocode. The major objective of the pseudocode is to compute the branch-transformer margin in an LV network.

Pseudocode to determinebranch-transformer margin

1. Start;
2. Perform a power flow analysis in the absence of a solar PV unit in the LV network;
3. Locate and position a solar PV unit at the lowest voltage bus, below 0.95 p.u;
4. Perform a power flow analysis for the LV network;
5. Identify branches with RPF and observe values of $P^{\mathrm{B}}_{\mathrm{net}}$ (t) and P_{Tx} (t);
6. If $P^{B}_{net}\,(t) = 0$ then go to step 10;
7. Else IF P_{Tx} (t) $= 0$ then go to step 11;
8. Else Repeat steps 3 to 5;
9. Compute total accumulated solar injected kVA as branch-based maximum depth of penetration, $D_{\mathrm{B\,max}}$;

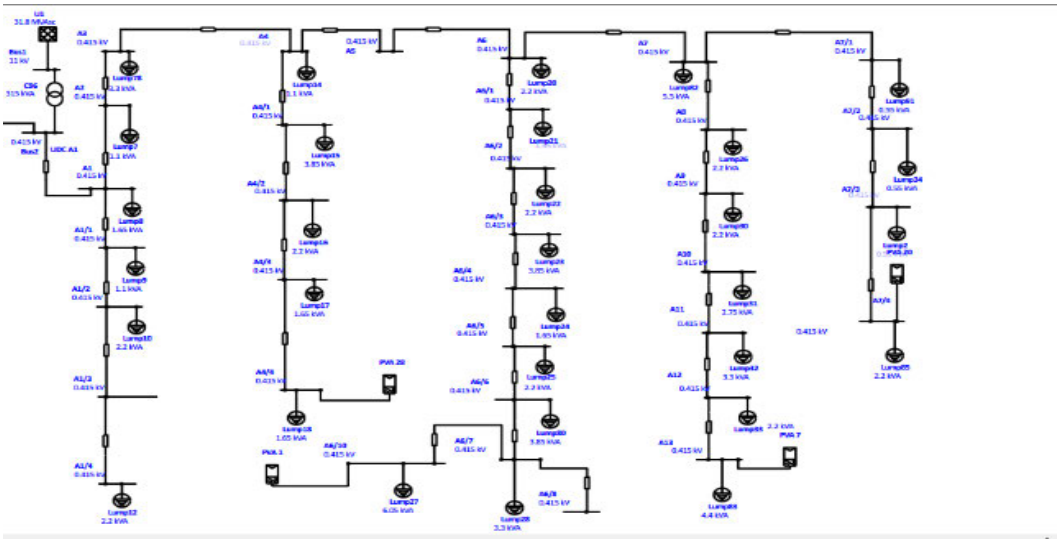

FIGURE 6. Single-line schematic showing a section of the solar PV-integrated ECG-LV Network.

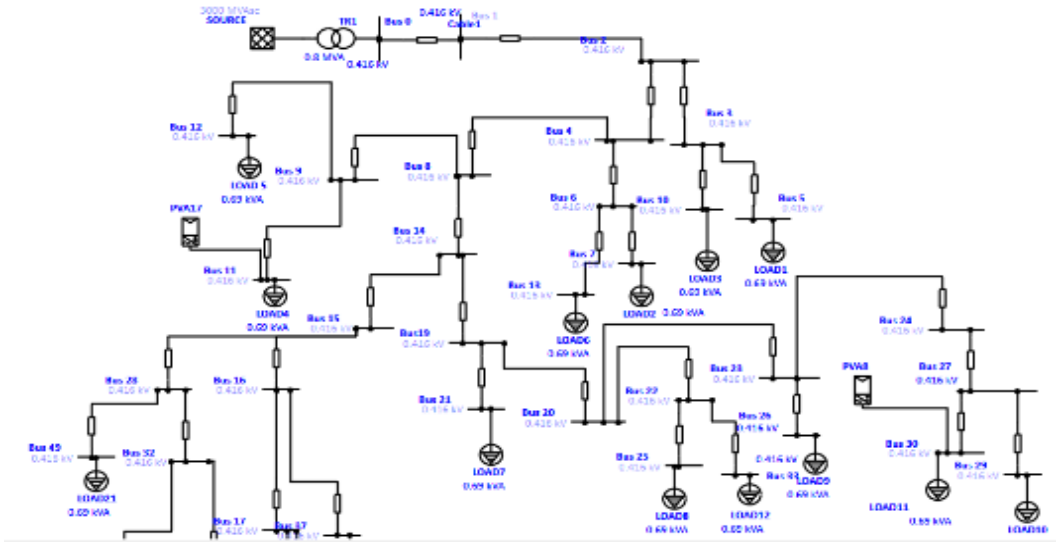

FIGURE 7. Single-line schematic showing a section of the solar PV-integrated modified IEEE LV European test network.

10. Compute total accumulated solar injected kVA as branch-based maximum depth of penetration, D_{Txmax};
11. Compute Branch-Transformer RPF Margin = ($D_{Tx\ max} - D_{B\ max}$);
12. Stop.

III. RESULTS AND DISCUSSIONS

This section explores in detail the results of the simulations for both the modified IEEE European test network and the ECG LV network. There has been a considerable increase in studies concerning network feeder power dynamics on line loading conditions due to RPF which is caused by increased PV penetrations. Among the most notable are the works of [13], [31], and [39]. However, extensions to these previous works, as presented in this study, involve a holistic approach to studying the power flow dynamics in the branch lines due to PV penetration in the LV networks.

Results from the simulation studies are used to create statistical models to quantify the impact of PV penetration on key branch parameters such as APF, line loading, and kW losses. The models will predict violations in the line loadings, and the RPF and estimate the maximum penetration depth of solar PV in the network.

These findings are significant in the determination of pre-determined critical parameters to safeguard the network against line overload due to RPF caused by excessive solar PV deployments. It is established from the simulation results that the RPF occurs randomly in the network branches. The paths of these hot spot branches are moving targets that depend on the power flow dynamics between adjacent branches,

TABLE 9. Simulation results for solar PV integrated ECG LV network.

Cumulative Solar PV Penetrations	Solar PV Penetration (kVA)	Solar PV Penetration (%)	Net Branch APF (kW)	Ave. Branch Loading (%)	No. of Branches with RPF	Ave. Branch APF Flow (kW)	Total Losses (kW)	Transformer APF (kW)
PV-0	0	0	1149.23	9.58	0	14.36	13.06	144.6
PV-1	19.93	12	898.25	8.3	7	12.13	9.33	121.8
PV-2	39.86	24	682.35	7.57	11	10.55	7.57	101.2
PV-3	59.79	36	515.45	6.79	14	9.06	5.30	79.56
PV-4	79.72	48	316.88	6.19	20	7.84	4.00	61.01
PV-5	99.65	60	94.19	6.3	29	7.21	3.79	40.58
PV-6	119.58	72	-143.5	6.83	38	7.47	4.24	21.01
PV-7	139.51	84	-489.12	7.44	56	8.04	4.91	2.64
PV-8	159.44	96	-640.54	7.82	62	9.35	5.39	-15.92
PV-9	179.37	108	-799.97	8.37	63	11.29	6.04	-34.29

TABLE 10. Simulation results for solar PV integrated modified IEEE LV European test network.

Cumulative solar PV Penetrations	Solar PV Penetration (kVA)	Solar PV Penetration (%)	Net Branch APF (kW)	Ave. Branch Loading (%)	No. of Branches with RPF	Ave. Branch APF Flow (kW)	Total Losses (kW)	Transformer APF (kW)
PV-0	0	0	1435.57	9.05	0	12.48	16.52	110.6
PV-1	19.93	15	1185.62	8.95	5	11.24	15.83	107.9
PV-2	39.86	31	764	8.1	14	9.44	11.65	85.75
PV-3	59.79	46	397.1	7.46	22	7.74	8.81	64.51
PV-4	79.72	61	47.88	7.32	31	7.28	7.90	45.3
PV-5	99.65	77	-244.76	7.52	37	7.82	7.96	26.78
PV-6	119.58	92	-452.71	7.48	45	7.33	7.76	7.56
PV-7	139.51	107	-659.11	7.69	53	8.38	8.04	-11.17
PV-8	159.44	123	-771.38	7.87	55	9.21	8.39	-30

the level of PV penetration, and the loads drawing current through the branches.

The stochastic nature of these activities makes it difficult to establish global solutions that will account for the individual contributions of network branches exposed to RPF due to the high solar PV impact. Hence, this study proposes non-trivial solutions such as net and average values of key parameters for network branch assessment. A consequence of this study is the establishment of a branch-transformer RPF safe margin, beyond which RPF will flow into the substation transformer. The modeled networks in Figure 6 and Figure 7 show the grid-tied solar PV test networks. The summary results of simulations for the studies are presented in Table 9 and Table 10.

The two LV networks used as case studies have considerable differences in the following: (a) Loadings and load patterns in transformer systems and (b) solar PV dimensions and step sizes. Nevertheless, the results obtained for these networks are expected to follow similar patterns. Each of the key results obtained will now be discussed in the following sections.

A. ANALYSIS OF BRANCH OPERATING PARAMETERS

In the sections that follow, simulation data from the two networks were utilized to generate statistical graphs and models illustrating the correlation between PV penetration and key network branch parameters.

1) ACTIVE POWER FLOW

Results for net active power and average active power at the branches per penetration are presented in Figures 8 and 9 respectively. The graphs in Figure 8, show that the net branch APF involves sign changes at the zero-crossing into the RPF mode [68], [75]. Theoretically, it is expected that RPF flows only beyond the zero-crossing point. However, the results of the study showed that fewer branches in both networks exhibit negative signs in their active power, showing RPF before the net active power zero-crossing point is reached. In Figure 9, it is possible to see the average APF decreasing to a minimum with increased penetration in both networks.

Beyond this minimum value, significant RPF is developed in the branches. This result is comparable to the findings in [1], where RPF is established beyond a minimum value of the curve as PV penetration increases. Using a time-series equivalent to the depth of penetration, authors in [76] obtained comparable results for the active power at both the substation and feeder levels in an LV system for the scenario in Figure 9. This shows that increased PV penetrations potentially increase the RPF events in the branches, and ultimately reverse the power flow into the substation transformer.

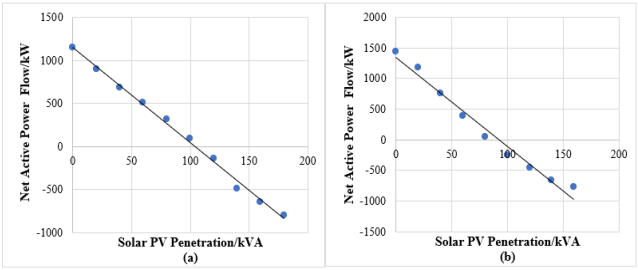

FIGURE 8. Net active power flow for (a) ECG LV network (b) modified IEEE European test network.

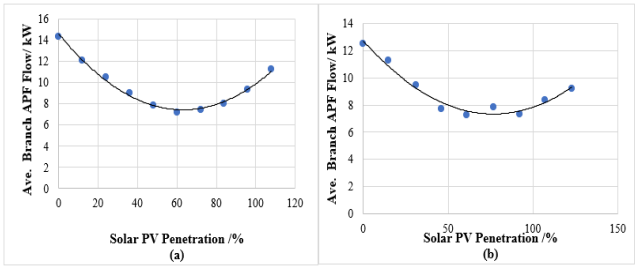

FIGURE 9. Average branch active power flow in (a) ECG LV network (b) modified IEEE European test network.

2) NETWORK BRANCHES WITH RPF

Figure 10 shows how the number of branches with RPF increases with an increase in PV penetration in both networks. From the results, it is possible to have fewer lines exhibiting RPF without violating the voltage limit [27]. In both networks, fewer branches exhibit RPF at lower penetration levels.

For instance, it is observed from Figures 10(a) and 10(b) that for the same penetration level PV-3 (equivalent to 59.79 kVA), there are 14 and 22 branches with RPF in the networks respectively. This difference is expected for reasons of different network features discussed in the introduction to this section. Additionally, the modified IEEE European test network consists of light loads subjecting the network to more cases of RPF with more PV penetrations [77]. What is more important is that the general pattern of an increased number of branches with RPF due to high PV penetration is established in both networks.

It is worth noting that significant RPF flows in each of the networks before maximum penetration depth is reached. Furthermore, a few individual branches may be subjected to RPF, even though their net contribution may not reverse power into the transformer.

For instance, at a penetration of 48% in the ECG network, 20 branches register RPF. However, at this penetration level, the transformer, which is operating at 61 kW, does not register RPF (Table 9). These results are supported by [19], who investigated the increased number of RPF events half-hourly on a feeder due to PV penetration.

3) LINE LOADINGS

Line loading is a function of the continuous operating current of the line expressed as a percentage of the conductor

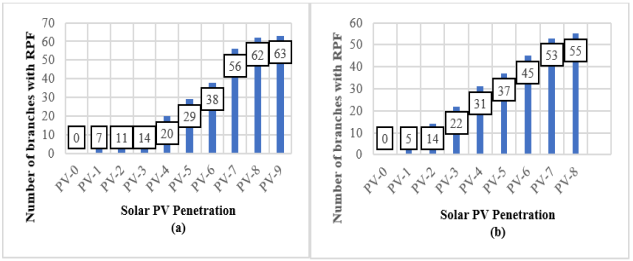

FIGURE 10. Branch conductors with RPF for (a) ECG LV network (b) modified IEEE European test network.

ampacity. The thermal current rating of the conductors is the primary limiting factor in the LV network's capacity to handle power flow with PV penetration [34], [40]. In Figures 11 (a) and 11 (b), the profiles for the average branch loading per PV penetration are shown. It is observed that the PV penetration will initially reduce the loading level of an increased number of branches, freeing up capacity on the lines.

As the penetration increases, most of the branches are subjected to reduced thermal stress resulting in a minimum average branch loading. From Figure 10, there is evidence that isolated RPF branches exist, giving rise to a few cases of an increased number of overloads on the branches. Figure 11 shows that beyond the minimum points in both graphs, increased loadings are recorded in the branches, resulting in an increased average branch loading per penetration. However, sustained PV penetration will potentially overload the branches beyond their thermal capacities (20). Similar findings have been reported in the works of [28], [29], and [42] for thermally constrained network conductors as a result of increased PV penetration. Thermally constrained lines due to overload potentially, lose their tensile stress and suffer from thermal aging [78]. Therefore, when designing the network, planners must take into account how PV penetration will impact the loading parameters of transmission lines [68].

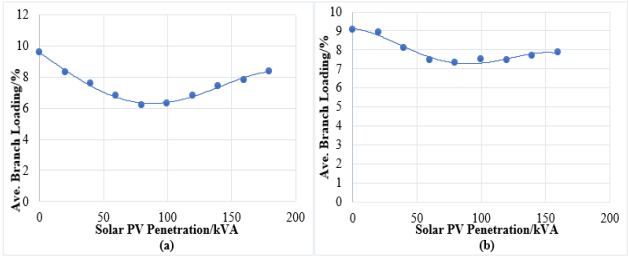

FIGURE 11. Average branch loading for (a) ECG LV network (b) modified IEEE European test network.

4) LINE POWER LOSSES

Power losses in the network branches are affected by the level of solar PV penetration. The total branch losses per PV penetration are presented in Figure 12. In both networks, at low

PV penetrations, capacity is freed as less current is drawn from the grid which results in low branch losses. At high penetrations, which results in high PV generation, lines are overloaded due to RPF (20). The resulting increase in line current increases the line losses. The following are observed from Figures 12 (a) and 12 (b): At the initial stage, the total losses decrease from 13.06 kW and 16.52 kW to a minimum of 3.79 kW and 7.82 kW respectively in both networks.

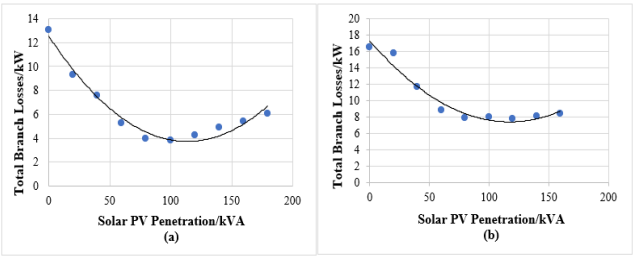

FIGURE 12. Total branch losses (a) ECG LV network (b) Modified IEEE European test network.

Further increase in PV penetration levels results in RPF overloading and increasing the branch currents. Therefore, the total branch losses increase beyond the minimum total losses. These results support the findings of [31], who investigated network system losses as a result of high PV injection into the network. Similar results are reported in the works of [13], [72], and [79].

B. EFFECTS OF HIGH PV PENETRATION ON THREE-PHASE LOADS

Three-phase load configurations in an LV network can be balanced or unbalanced depending on the variations in customer load demand [80], [81]. These load configurations respond differently to high PV penetrations which affect the overload conditions of the lines feeding the loads. For instance, for the same three-phase PV inverter power injected into the network, load currents are equally distributed in a balanced three-phase system. However, different load currents are drawn by an unbalanced three-phase load configuration. Particularly with sustained PV penetration, reverse power flows occur in the low-load phase, causing thermal violations in that phase [82]. Therefore, unbalanced three-phase loads may violate power quality standards such as voltage and line loading, and cause significant protection problems in the affected phase due to RPF [83]. Studies on unbalanced load scenarios with DGs are well documented in the literature [80], [84], [85], [86]. In the present study, the ECG network featured unbalanced loads which were modeled as lumped three-phase loads without compromising study analysis. The influence of these lumped three-phase loads on the average branch loading is considered in the branch threshold analysis.

C. NETWORK BRANCH THRESHOLD ANALYSIS

To establish global controls for key parameters on the LV network branches due to PV penetration, it is necessary to consider unified branch network threshold evaluation. Table 11 presents the branch threshold criteria for the two networks based on the predictive models in (21) and (22), (23) and (24), and (25) and (26) which were created from the simulation results. In Table 11, the estimated branch limits for the modified IEEE European test network and the ECG LV network are compared. Equations (21) and (22) are two models for the net branch active power, P^{B}_{net} obtained from Figure 8 to predict the depth of penetration, D (% or kVA) at the zero-crossing point.

$$\text{ECG network: } P^{\text{B}}_{\text{net}} = -11.06 \cdot D + 1150.3 \tag{21}$$

$$\text{IEEE test network: } P^{\text{B}}_{\text{net}} = -14.582 \cdot D + 1351.6 \tag{22}$$

According to (21), the maximum penetration depth at the zero crossing point is 62.6% in the ECG network and 69.8% in the IEEE test network. Similarly, in Figure 9, we obtain models for the average active power flow in the branches, $P^{\text{ave}}_{\text{br}}$ for the two networks, presented in (23) and (24) to predict the RPF in the ECG network and IEEE test network respectively.

$$\text{ECG network: } P^{\text{ave}}_{\text{br}} = 0.0007 \cdot D^2 - 0.1369 \cdot D + 14.617 \tag{23}$$

$$\text{IEEE test network: } P^{\text{ave}}_{\text{br}} = 0.0005 \cdot D^2 - 0.1086 \cdot D + 12.735 \tag{24}$$

For instance, given the depth of PV penetration, these models predict the average active power flow in the branches, which determines the RPF. For instance, in the IEEE test network, the RPF is estimated to be 7.36 kW using (24). This represents the maximum branch active power flow obtained at a maximum allowable penetration of 69.8%. In Table 11 it is observed that these values are lower than the estimated values for the ECG network. This is because the IEEE test network is a low-load network, therefore penetration level is higher, and reverse current develops easily with relatively low active power [87]. These models can be related to the findings in [1], which used a similar model to estimate the average total reverse power flow under the impact of PV penetration in a given distribution network.

TABLE 11. Summary of net branch limits for RPF.

Network	Solar PV Max. Penetration (%)	Max. Average Branch APF (kW)	Max. Average Branch Loading (%)	Total Branch Losses (kW)
ECG LV Network	62.6 (104 kVA)	7.44	6.42	3.79
Modified IEEE European Test Network	69.8 (92.69 kVA)	7.36	7.28	7.82

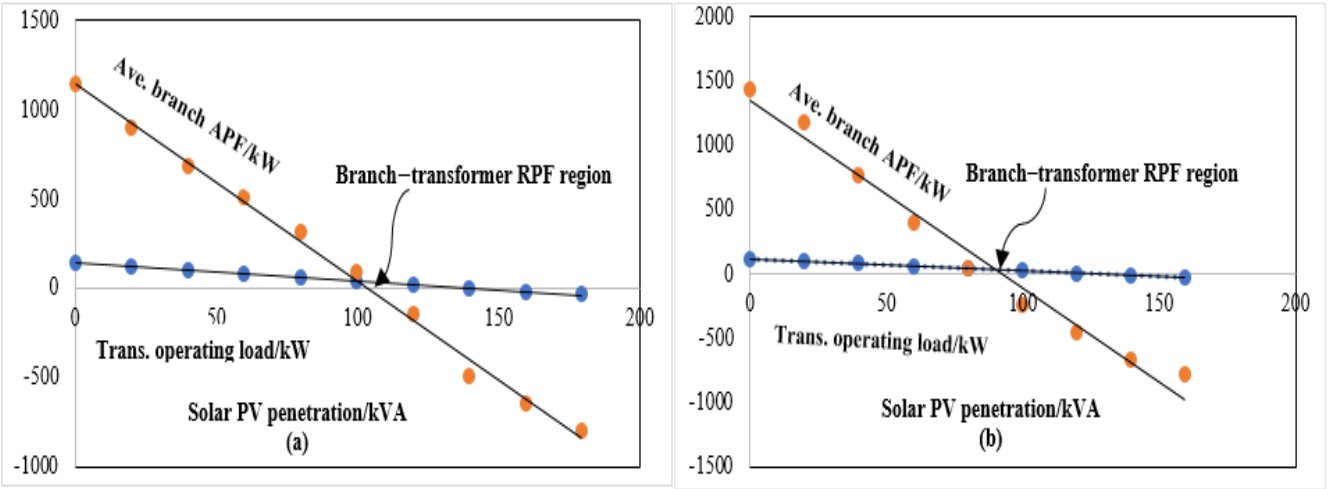

FIGURE 13. Transformer operating load and average branch APF per PV penetration showing transformer-branch region for (a) ECG LV network (b) modified IEEE European test network.

Correlation models obtained for the two networks in Figure 11 are presented in (25) and (26).

$$\text{ECG network: } L_{\text{br}}^{\text{ave}} = -2{\cdot}10^{-8}{\cdot}D^4+6{\cdot}10^{-6}{\cdot}D^3 -0.0002{\cdot}D^2-0.0541{\cdot}D+9.5433 \quad (25)$$

$$\text{IEEE test network: } L_{\text{br}}^{\text{ave}} = -3{\cdot}10^{-8}{\cdot}D^4+1{\cdot}10^{-5}{\cdot}D^3 -0.0008{\cdot}D^2-0.0048{\cdot}D+9.1162 \quad (26)$$

The models represent the average branch loading, $L_{\text{br}}^{\text{ave}}$ measured in percentage of the average branch operating current. Estimates of the average loading conditions of the network branches due to PV penetration can be determined using these models. At the maximum penetration depth, the average branch loading is 6.42% (Average current=16.7 A) and 7.28% (Average current=18.1 A) as observed in the ECG and IEEE test networks respectively (Table 9). These results are expected since low-load networks are more susceptible to RPF and hence, greater thermal stress. This is the case with the IEEE test network. We conclude that even though these lines have not reached their thermal limits at these rates, they will exhibit significant RPF at depths beyond the maximum penetration depth. However, in [13], the authors investigated penetration limits on transmission lines and determined that rather, the line thermal limits placed restrictions on the maximum penetration depth. Therefore, a good planning strategy for utilities is to determine the penetration level beyond which the branches will reach their thermal capacities.

Closely related to the line overload conditions is the total branch losses per PV penetration. Overloaded branches are thermally stressed due to RPF from excess solar PV generation [66]. These high currents result in high branch losses. In this study, we have seen how excess PV penetration contributes to branch losses. For instance, the IEEE test network registers a total minimum branch loss of 7.28 kW at the maximum penetration depth. It is observed in Figures 12 (a) and 12 (b) that excess PV injection increases the branch losses because of an increase in RPF events that overload the branches.

Details of the total minimum branch losses corresponding to the maximum penetration depth in the ECG network are shown in Table 11. The study shows that a loss management strategy is essential because RPF can increase total losses in branches with high PV penetration. A loss management scheme, similar to the scheme in the present study, for managing PV-grid integration challenges is found in the following works: [88], [89], and [90].

D. ASSESSMENT OF NETWORK BRANCH-TRANSFORMER RPF MARGIN

The safe margin represents additional penetration depth, beyond which RPF progresses into the substation transformer. In this region of branch-transformer RPF margin, there may not be adverse effects on the protection systems at the substation [91]. However, beyond this region, the substation transformer is subjected to RPF similar to the situations in the following studies: [92], [93], and [94]. Figure 13 shows the relationship between the average branch active power and the transformer operating active power under increased PV penetration. Simulation results show that the transformer delays in exhibiting RPF more than the network branches. This situation creates the branch-transformer RPF region. The transformer-based maximum PV penetration depths are predicted from the models in (27) and (28) obtained from Figure 13.

$$\text{ECG network: } P_{\text{TX}} - 0.9922 \cdot D + 141.21 \quad (27)$$

$$\text{IEEE test network: } P_{\text{TX}} = -0.9314 \cdot D + 119.5 \quad (28)$$

The models estimate the maximum penetration levels as 85.7% and 96.6% in the ECG LV network and the modified IEEE European test network respectively. It is obvious from

Table 9 that these limits exceed the branch-based limits corresponding to each network.

In Figure 13(a) for instance, the network branches develop significant RPF at a maximum penetration depth of 62.6% before the substation transformer develops RPF at a depth of 85.7%. So, a deficit of 23.1% is what represents the branch-transformer RPF region (18). A similar region of 26.8% is represented in the case of Figure 13 (b) where the maximum penetration depths of 69.8% and 96.6% are recorded at RPF margins in the network branches and the substation transformer respectively. Table 12 presents a summary of the branch-transformer RPF margins expressed in percentage and apparent power (kVA) of the PV penetration for the two networks.

It is expected that conditions beyond the branch-transformer RPF region can lead to transformer tripping and prompt disconnect issues due to excessive relay operations [53], [66]. This phenomenon may also cause age deterioration in the transformer [95], [96].

These results are important for setting pre-determined critical parameters to protect the network branches from line overload due to RPF caused by excessive solar PV penetrations. In addition, critical stages of RPF require interventions such as those suggested in the study [94] and [97] where energy storage systems are installed close to the substation transformer to deal with excess power due to RPF.

TABLE 12. Summary of network branch-transformer RPF margins.

Test Network	Unit	Maximum values for penetration depths at the margin of RPF		Safe Margin of RPF
		Transformer	Network Branch	
ECG LV	%	85.70	62.60	23.1
Network	kVA	142.32	104.01	38.31
IEEE LV	%	96.60	69.80	26.80
Network	kVA	128.30	92.69	35.61

IV. CONCLUSION

This study presents an assessment of reverse power flow on line overload conditions under increased solar PV penetration in LV networks. Modeling, simulations, and statistical models are used to obtain the presented results. The average values for the RPF and the line overload at solar PV maximum penetration are estimated by the predictive models created from the simulation data. Results also show that the minimum total branch losses are obtained at the maximum PV penetration.

Furthermore, the detection of a significant number of branches with RPF per PV penetration shows that line overload may not be reached before RPF causes significant net power flow in the branches. Finally, a branch-transformer region is determined as a safe margin to protect the transformer from reverse power flow.

The approach used in this study faces several challenges which could be addressed in future works. They are as follows:

1. In this study, only the active power has been taken into consideration. One of the reasons is that household customers consume more active power than reactive power.
2. The solar PV output remained fixed in this investigation. Instead of a fixed value for the production during the worst case, a stochastic model could also be considered to take into account the solar radiation and seasonal changes that could affect solar PV production.
3. Loads are modeled as static and do not consider their statistical variation to seasonal changes that affect their load profile. This deterministic approach also modeled the household load for the worst-case scenario of maximum demand.
4. Issues concerning protection, coordination, and power quality, which are not addressed in this study, may limit PV penetration.

The proposed procedure outlined in this study establishes pre-determined critical parameters to protect LV network branches from line overload due to RPF caused by excessive solar PV installations. Therefore, it is vital to conduct studies that will aid engineers in planning systems with high PV penetration levels to determine the critical PV penetration levels for a given network. A similar procedure could be adopted in the Ghanaian LV networks, where PV solar impact studies are currently gaining traction. Also, the economic and financial aspects of the studies can be considered for future work.

Furthermore, network operators should use data from their networks to estimate the key parameters of the branches when making assessments of RPF as part of their distribution system planning. In this study, the specific results are only valid for the studied networks, but the method itself has broader applications.

REFERENCES

[1] H. Sadeghian and Z. Wang, "A novel impact-assessment framework for distributed PV installations in low-voltage secondary networks," *Renew. Energy*, vol. 147, pp. 2179–2194, Mar. 2020, doi: 10.1016/j.renene.2019.09.117.

[2] M. Z. U. Abideen, O. Ellabban, S. S. Refaat, H. Abu-Rub, and L. Al-Fagih, "A novel methodology to determine the maximum PV penetration in distribution networks," in *Proc. 2nd Int. Conf. Smart Grid Renew. Energy (SGRE)*, Nov. 2019, pp. 1–6, doi: 10.1109/SGRE46976.2019.9020948.

[3] S. Freitas, T. Santos, and M. C. Brito, "Impact of large scale PV deployment in the sizing of urban distribution transformers," *Renew. Energy*, vol. 119, pp. 767–776, Apr. 2018, doi: 10.1016/j.renene.2017.10.096.

[4] S. Shivashankar, S. Mekhilef, H. Mokhlis, and M. Karimi, "Mitigating methods of power fluctuation of photovoltaic (PV) sources—A review," *Renew. Sustain. Energy Rev.*, vol. 59, pp. 1170–1184, Jun. 2016, doi: 10.1016/j.rser.2016.01.059.

[5] S. M. M. Agah and H. A. Abyaneh, "Quantification of the distribution transformer life extension value of distributed generation," *IEEE Trans. Power Del.*, vol. 26, no. 3, pp. 1820–1828, Jul. 2011, doi: 10.1109/TPWRD.2011.2115257.

[6] M. A. Cohen and D. S. Callaway, "Effects of distributed PV generation on California's distribution system, Part 1: Engineering simulations," *Sol. Energy*, vol. 128, pp. 126–138, Apr. 2016, doi: 10.1016/j.solener.2016.01.002.

[7] P. Jahangiri and D. C. Aliprantis, "Distributed Volt/VAr control by PV inverters," *IEEE Trans. Power Syst.*, vol. 28, no. 3, pp. 3429–3439, Aug. 2013, doi: 10.1109/TPWRS.2013.2256375.
[8] D. Cheng, B. A. Mather, R. Seguin, J. Hambrick, and R. P. Broadwater, "Photovoltaic (PV) impact assessment for very high penetration levels," *IEEE J. Photovolt.*, vol. 6, no. 1, pp. 295–300, Jan. 2016, doi: 10.1109/JPHOTOV.2015.2481605.
[9] S. Arora, S. Kaur, and R. Khanna, "A review on voltage challenges and remedial methods with excessive PV penetration in radial distribution feeder," in *Proc. 5th Int. Conf. Signal Process., Comput. Control (ISPCC)*, Oct. 2019, pp. 47–52, doi: 10.1109/ISPCC48220.2019.8988454.
[10] C. T. Gaunt, E. Namanya, and R. Herman, "Voltage modelling of LV feeders with dispersed generation: Limits of penetration of randomly connected photovoltaic generation," *Electr. Power Syst. Res.*, vol. 143, pp. 1–6, Feb. 2017, doi: 10.1016/j.epsr.2016.08.042.
[11] O. Gandhi, D. S. Kumar, C. D. Rodríguez-Gallegos, and D. Srinivasan, "Review of power system impacts at high PV penetration Part I: Factors limiting PV penetration," *Sol. Energy*, vol. 210, pp. 181–201, Nov. 2020, doi: 10.1016/j.solener.2020.06.097.
[12] D. Cheng, B. Mather, R. Seguin, J. Hambrick, and R. P. Broadwater, "PV impact assessment for very high penetration levels," in *Proc. IEEE 42nd Photovoltaic Spec. Conf. (PVSC)*, Jun. 2015, pp. 1–6, doi: 10.1109/PVSC.2015.7356170.
[13] M. A. Talaq and C. A. Belhaj, "Optimal PV penetration for power losses subject to transient stability and harmonics," *Proc. Comput. Sci.*, vol. 175, pp. 508–516, Dec. 2020, doi: 10.1016/j.procs.2020.07.072.
[14] T. Olowu, A. Sundararajan, M. Moghaddami, and A. Sarwat, "Future challenges and mitigation methods for high photovoltaic penetration: A survey," *Energies*, vol. 11, no. 7, p. 1782, Jul. 2018, doi: 10.3390/en11071782.
[15] A. Anzalchi, A. Sundararajan, A. Moghadasi, and A. Sarwat, "High-penetration grid-tied photovoltaics: Analysis of power quality and feeder voltage profile," *IEEE Ind. Appl. Mag.*, vol. 25, no. 5, pp. 83–94, Sep. 2019, doi: 10.1109/MIAS.2019.2923104.
[16] D. McPhail, B. Croker, and B. Harvey, "A study of solar PV saturation limits for representative low voltage networks," in *Proc. Australas. Univ. Power Eng. Conf. (AUPEC)*, 2016, pp. 1–5.
[17] H. Al-Saadi, R. Zivanovic, and S. F. Al-Sarawi, "Probabilistic hosting capacity for active distribution networks," *IEEE Trans. Ind. Informat.*, vol. 13, no. 5, pp. 2519–2532, Oct. 2017, doi: 10.1109/TII.2017.2698505.
[18] A. Hoke, R. Butler, J. Hambrick, and B. Kroposki, "Steady-state analysis of maximum photovoltaic penetration levels on typical distribution feeders," *IEEE Trans. Sustain. Energy*, vol. 4, no. 2, pp. 350–357, Apr. 2013, doi: 10.1109/TSTE.2012.2225115.
[19] V. Sharma, S. M. Aziz, M. H. Haque, and T. Kauschke, "Effects of high solar photovoltaic penetration on distribution feeders and the economic impact," *Renew. Sustain. Energy Rev.*, vol. 131, Oct. 2020, Art. no. 110021, doi: 10.1016/j.rser.2020.110021.
[20] H. Mortazavi, H. Mehrjerdi, M. Saad, S. Lefebvre, D. Asber, and L. Lenoir, "A monitoring technique for reversed power flow detection with high PV penetration level," *IEEE Trans. Smart Grid*, vol. 6, no. 5, pp. 2221–2232, Sep. 2015, doi: 10.1109/TSG.2015.2397887.
[21] J. O. Petinrin and M. Shaabanb, "Impact of renewable generation on voltage control in distribution systems," *Renew. Sustain. Energy Rev.*, vol. 65, pp. 770–783, Nov. 2016, doi: 10.1016/j.rser.2016.06.073.
[22] A. Ameur, A. Berrada, K. Loudiyi, and M. Aggour, "Analysis of renewable energy integration into the transmission network," *Electr. J.*, vol. 32, no. 10, Dec. 2019, Art. no. 106676, doi: 10.1016/j.tej.2019.106676.
[23] F. Ebe, B. Idlbi, J. Morris, G. Heilscher, and F. Meier, "Evaluation of PV hosting capacities of distribution grids with utilisation of solar roof potential analyses," *Open Access Proc. J.*, vol. 2017, no. 1, pp. 2265–2269, Oct. 2017, doi: 10.1049/oap-cired.2017.0848.
[24] E. Mulenga, M. H. J. Bollen, and N. Etherden, "Distribution networks measured background voltage variations, probability distributions characterization and solar PV hosting capacity estimations," *Electr. Power Syst. Res.*, vol. 192, Mar. 2021, Art. no. 106979, doi: 10.1016/j.epsr.2020.106979.
[25] Y. T. Tan and D. S. Kirschen, "Impact on the power system of a large penetration of photovoltaic generation," in *Proc. IEEE Power Eng. Soc. Gen. Meeting*, Jun. 2007, pp. 1–8, doi: 10.1109/PES.2007.385563.
[26] W. K. Yap, L. Havas, E. Overend, and V. Karri, "Neural network-based active power curtailment for overvoltage prevention in low voltage feeders," *Expert Syst. Appl.*, vol. 41, no. 4, pp. 1063–1070, Mar. 2014, doi: 10.1016/j.eswa.2013.07.103.
[27] F. H. M. Rafi, M. J. Hossain, and J. Lu, "Hierarchical controls selection based on PV penetrations for voltage rise mitigation in a LV distribution network," *Int. J. Elect. Power Energy Syst.*, vol. 81, pp. 123–139, Oct. 2016, doi: 10.1016/j.ijepes.2016.02.013.
[28] J. P. Holguin, D. C. Rodriguez, and G. Ramos, "Reverse power flow (RPF) detection and impact on protection coordination of distribution systems," *IEEE Trans. Ind. Appl.*, vol. 56, no. 3, pp. 2393–2401, May 2020, doi: 10.1109/TIA.2020.2969640.
[29] D. S. Nair and T. Rajeev, "Impact of reverse power flow due to high solar PV penetration on distribution protection system," in *Sustainable Energy and Technological Advancements*. Singapore: Springer, 2022, doi: 10.1007/978-981-16-9033-4_1.
[30] M. Katsanevakis, R. A. Stewart, and J. Lu, "Energy storage system utilisation to increase photovoltaic penetration in low voltage distribution feeders," *J. Energy Storage*, vol. 14, pp. 329–347, Dec. 2017, doi: 10.1016/j.est.2017.07.022.
[31] C. H. Tie, C. K. Gan, K. A. Ibrahim, and M. Shamshiri, "Probabilistic evaluation of the impact of residential photovoltaic system on Malaysia low-voltage network using Monte Carlo approach," *J. Renew. Sustain. Energy*, vol. 7, no. 6, Nov. 2015, Art. no. 063110, doi: 10.1063/1.4936297.
[32] A. Navarro-Espinosa and L. F. Ochoa, "Probabilistic impact assessment of low carbon technologies in LV distribution systems," *IEEE Trans. Power Syst.*, vol. 31, no. 3, pp. 2192–2203, May 2016, doi: 10.1109/TPWRS.2015.2448663.
[33] E. Zio, M. Delfanti, L. Giorgi, V. Olivieri, and G. Sansavini, "Monte Carlo simulation-based probabilistic assessment of DG penetration in medium voltage distribution networks," *Int. J. Electr. Power Energy Syst.*, vol. 64, pp. 852–860, Jan. 2015, doi: 10.1016/j.ijepes.2014.08.004.
[34] S. Bossart and R. Staubly. (2014). *Dynamic Line Rating Systems for Transmission Lines*. [Online]. Available: https://www.smartgrid.gov/files/SGDP_Transmission_DLR_Topical_Report_04-25-14_FINAL.pdf
[35] J. Heckenbergerova, P. Musilek, and K. Filimonenkov, "Assessment of seasonal static thermal ratings of overhead transmission conductors," in *Proc. IEEE Power Energy Soc. Gen. Meeting*, Mar. 2011, pp. 1–4, doi: 10.1109/PES.2011.6039393.
[36] L. Wenbo, F. Shanqiang, L. Huadong, J. Zhe, and C. Bo, "Daily thermal rating calculation of overhead conductor driven by meteorological data," in *Proc. 10th Int. Conf. Commun., Circuits Syst. (ICCCAS)*, 2018, pp. 79–83, doi: 10.1109/ICCCAS.2018.8768928.
[37] P. Schell, "Dynamic line rating (DLR): A safe, quick, and economic way to transition power networks towards renewable energy," in *Renewable Energy Integration: Practical Management of Variability, Uncertainty, and Flexibility in Power Grids*, Lawrence E. Jones, pp. 405–411, doi: 10.1016/B978-0-12-407910-6.00032-6.
[38] D. Almeida, S. Abeysinghe, M. P. Ekanayake, R. I. Godaliyadda, J. Ekanayake, and J. Pasupuleti, "Generalized approach to assess and characterise the impact of solar PV on LV networks," *Int. J. Electr. Power Energy Syst.*, vol. 121, Oct. 2020, Art. no. 106058, doi: 10.1016/j.ijepes.2020.106058.
[39] R. A. Shayani and M. A. G. de Oliveira, "Photovoltaic generation penetration limits in radial distribution systems," *IEEE Trans. Power Syst.*, vol. 26, no. 3, pp. 1625–1631, Aug. 2011, doi: 10.1109/TPWRS.2010.2077656.
[40] D. Enescu, P. Colella, A. Russo, R. F. Porumb, and G. C. Seritan, "Concepts and methods to assess the dynamic thermal rating of underground power cables?" *Energies*, vol. 14, no. 9, pp. 1–23, 2021, doi: 10.3390/en14092591.
[41] O. Rahman, K. M. Muttaqi, and D. Sutanto, "Three phase power flow analysis of distribution network performance with high penetration of single phase PV units integrated with energy storage system," in *Proc. Australas. Universities Power Eng. Conf. (AUPEC)*, Nov. 2018, pp. 1–18, doi: 10.1109/AUPEC.2018.8758001.
[42] A. Abbas, M. S. Khalid, A. Mughees, A. Mughees, S. Yousaf, F. Sohail, and H. Rehman, "Monitoring and control of reverse feed current in grid tied PV systems using multiple MPPT inverter," in *Proc. IEEE 23rd Int. Multitopic Conf. (INMIC)*, Nov. 2020, pp. 3–8, doi: 10.1109/INMIC50486.2020.9318165.
[43] S. Kadam, B. Bletterie, and W. Gawlik, "A large scale grid data analysis platform for DSOs," *Energies*, vol. 10, no. 8, p. 1099, Jul. 2017, doi: 10.3390/en10081099.
[44] S. J. Steffel, P. R. Caroselli, A. M. Dinkel, J. Q. Liu, R. N. Sackey, and N. R. Vadhar, "Integrating solar generation on the electric distribution grid," *IEEE Trans. Smart Grid*, vol. 3, no. 2, pp. 878–886, Jun. 2012, doi: 10.1109/TSG.2012.2191985.

[45] J. D. Watson, N. R. Watson, D. Santos-Martin, A. R. Wood, S. Lemon, and A. J. V. Miller, "Impact of solar photovoltaics on the low-voltage distribution network in New Zealand," *IET Gener., Transmiss. Distrib.*, vol. 10, no. 1, pp. 1–9, Jan. 2016, doi: 10.1049/iet-gtd.2014.1076.

[46] M. Thomson and D. G. Infield, "Impact of widespread photovoltaics generation on distribution systems," *IET Renew. Power Gener.*, vol. 1, no. 1, pp. 33–40, Mar. 2007, doi: 10.1049/iet-rpg:20060009.

[47] G. Matkar, D. K. Dheer, A. S. Vijay, and S. Doolla, "A simple mathematical approach to assess the impact of solar PV penetration on voltage profile of distribution network," in *Proc. Nat. Power Electron. Conf. (NPEC)*, Dec. 2017, pp. 209–214, doi: 10.1109/NPEC.2017.8310460.

[48] G. De Carne, G. Buticchi, Z. Zou, and M. Liserre, "Reverse power flow control in a ST-fed distribution grid," *IEEE Trans. Smart Grid*, vol. 9, no. 4, pp. 3811–3819, Jul. 2018, doi: 10.1109/TSG.2017.2651147.

[49] P. Sudhakar, S. Malaji, and B. Sarvesh, "Reducing the impact of DG on distribution networks protection with reverse power relay," *Mater. Today, Proc.*, vol. 5, no. 1, pp. 51–57, 2018, doi: 10.1016/j.matpr.2017.11.052.

[50] J. Pollock and D. Hill, "Overcoming the issues associated with operating a distribution system in reverse power flow," in *Proc. IET Conf. Publ.*, 2016, pp. 2–7, doi: 10.1049/cp.2016.0552.

[51] I. B. Majeed and N. I. Nwulu, "Impact of reverse power flow on distributed transformers in a solar-photovoltaic-integrated low-voltage network," *Energies*, vol. 15, no. 23, p. 9238, Dec. 2022, doi: 10.3390/en15239238.

[52] A. Demazy, T. Alpcan, and I. Mareels, "A probabilistic reverse power flows scenario analysis framework," *IEEE Open Access J. Power Energy*, vol. 7, pp. 524–532, 2020, doi: 10.1109/OAJPE.2020.3032902.

[53] S. Rahman, H. Aburub, M. Moghaddami, and A. I. Sarwat, "Reverse power flow protection in grid connected PV systems," in *Proc. SoutheastCon*, Apr. 2018, pp. 3–7, doi: 10.1109/SECON.2018.8478882.

[54] R. Frost, L. Zieland, D. Sharafi, and J. Susanto, "Impact of reverse power flow in distribution feeders on under-frequency load shedding schemes," in *Proc. Int. Conf. Smart Grids Energy Syst. (SGES)*, Nov. 2020, pp. 100–104, doi: 10.1109/SGES51519.2020.00025.

[55] E. A. Kwofie, G. Mensah, and V. S. Antwi, "Post commission grid impact assessment of a 20 MWp solar PV grid connected system on the ECG 33 kV network in Winneba," in *Proc. IEEE PES/IAS PowerAfrica*, Aug. 2019, pp. 521–526, doi: 10.1109/PowerAfrica.2019.8928841.

[56] G. Eduful, K. Atanga, and D. Pulfrey, "Simulation study of stand-alone and grid-tied photovoltaic systems in Ghana," *Lect. Notes Eng. Comput. Sci.*, vol. 2242, pp. 184–190, Nov. 2021.

[57] E. A. Kwofie, G. Mensah, and E. K. Anto, "Determination of the optimal power factor at which DG PV should be operated," in *Proc. IEEE PES PowerAfrica*, Jun. 2017, pp. 391–395, doi: 10.1109/PowerAfrica.2017.7991256.

[58] M. Obeng, S. Gyamfi, N. S. Derkyi, A. T. Kabo-Bah, and F. Peprah, "Technical and economic feasibility of a 50 MW grid-connected solar PV at UENR Nsoatre campus," *J. Cleaner Prod.*, vol. 247, Feb. 2020, Art. no. 119159, doi: 10.1016/j.jclepro.2019.119159.

[59] A. Kharrazi, V. Sreeram, and Y. Mishra, "Assessment techniques of the impact of grid-tied rooftop photovoltaic generation on the power quality of low voltage distribution network—A review," *Renew. Sustain. Energy Rev.*, vol. 120, Mar. 2020, Art. no. 109643, doi: 10.1016/j.rser.2019.109643.

[60] S. Somkun and V. Chunkag, "Unified unbalanced synchronous reference frame current control for single-phase grid-connected voltage-source converters," *IEEE Trans. Ind. Electron.*, vol. 63, no. 9, pp. 5425–5436, Sep. 2016.

[61] M. Dursun and M. K. Dosoglu, "LCL filter design for grid connected three-phase inverter," in *Proc. 2nd Int. Symp. Multidiscip. Stud. Innov. Technol.*, Oct. 2018, pp. 56–78, doi: 10.1109/ISMSIT.2018.8567054.

[62] *IEEE Standard for Interconnection and Interoperability of Distributed Energy Resources with Associated Electric Power Systems Interfaces*, IEEE Standard 1547, 2018.

[63] K. Ma, R. Li, and F. Li, "Utility-scale estimation of additional reinforcement cost from three-phase imbalance considering thermal constraints," *IEEE Trans. Power Syst.*, vol. 32, no. 5, pp. 3912–3923, Sep. 2017, doi: 10.1109/TPWRS.2016.2639101.

[64] M. E. Baran, H. Hooshyar, Z. Shen, and A. Huang, "Accommodating high PV penetration on distribution feeders," *IEEE Trans. Smart Grid*, vol. 3, no. 2, pp. 1039–1046, Jun. 2012, doi: 10.1109/TSG.2012.2190759.

[65] K. N. Bangash, M. E. A. Farrag, and A. H. Osman, "Manage reverse power flow and fault current level in LV network with high penetration of small scale solar and wind power generation," in *Proc. 53rd Int. Universities Power Eng. Conf. (UPEC)*, Sep. 2018, pp. 1–6, doi: 10.1109/UPEC.2018.8541923.

[66] P. Mohammadi and S. Mehraeen, "Challenges of PV integration in low-voltage secondary networks," *IEEE Trans. Power Del.*, vol. 32, no. 1, pp. 525–535, Feb. 2017, doi: 10.1109/TPWRD.2016.2556692.

[67] K. P. Kirui, D. K. Murage, and P. K. Kihato, "Fuse-fuse protection scheme ETAP model for IEEE 13 node radial test distribution feeder," *Eur. J. Eng. Res. Sci.*, vol. 4, no. 9, pp. 224–234, Sep. 2019.

[68] M. A. Khan, N. Arbab, and Z. Huma, "Voltage profile and stability analysis for high penetration solar photovoltaics," *Int. J. Eng. Work.*, vol. 5, no. 5, pp. 109–114, 2018.

[69] M. A. Khan and B. P. Hayes, "A reduced electrically-equivalent model of the IEEE European low voltage test feeder," in *Proc. IEEE Power Energy Soc. Gen. Meeting (PESGM)*, Denver, CO, USA, 2022, pp. 1–5, doi: 10.1109/PESGM48719.2022.9916806.

[70] K. Petrou, A. T. Procopiou, L. Gutierrez-Lagos, M. Z. Liu, L. F. Ochoa, T. Langstaff, and J. M. Theunissen, "Ensuring distribution network integrity using dynamic operating limits for prosumers," *IEEE Trans. Smart Grid*, vol. 12, no. 5, pp. 3877–3888, Sep. 2021, doi: 10.1109/TSG.2021.3081371.

[71] K. Tsamaase, U. Moyo, I. Zibani, I. Ngebani, and P. Mahindroo, "Approximate mathematical model for load profiling and demand forecasting," *J. Electr. Electron. Eng.*, vol. 12, no. 5, pp. 29–34, 2017.

[72] A. Setiawan, A. D. Pranadi, and E. A. Setiawan, "Determination of optimal PV locations and capacity in radial distribution system to reduce power losses," *Energy Proc.*, vol. 156, pp. 384–390, Jan. 2019, doi: 10.1016/j.egypro.2018.11.108.

[73] R. Broderick, J. Williaams, and K. Munoz-Ramos, "Clustering methods and feeder selection for PV system impact analysis," EPRI, Washington, DC, USA, Tech. Rep., 3002002562, 2014.

[74] A. Y. Saber, T. Khandelwal, and A. K. Srivastava, "Fast feeder PV hosting capacity using swarm based intelligent distribution node selection," in *Proc. IEEE Power Energy Soc. Gen. Meeting (PESGM)*, Aug. 2019, pp. 54–67, doi: 10.1109/PESGM40551.2019.8973389.

[75] C. V. Silva and A. M. Guerra, "Practical PV hosting capacity determination using load factor of the distribution transformer," in *Proc. IEEE PES Transmiss. Distrib. Conf. Exhib.*, Sep. 2020, pp. 354–546, doi: 10.1109/TDLA47668.2020.9326136.

[76] D. Divan, R. Moghe, and H. Chun, "Managing distribution feeder voltage issues caused by high PV penetration," in *Proc. IEEE 7th Int. Symp. Power Electron. Distrib. Gener. Syst. (PEDG)*, Jun. 2016, pp. 15–20, doi: 10.1109/PEDG.2016.7527047.

[77] T. Alquthami, R. S. Kumar, and A. A. Shaikh, "Mitigation of voltage rise due to high solar PV penetration in Saudi distribution network," *Electr. Eng.*, vol. 102, no. 2, pp. 881–890, Jun. 2020, doi: 10.1007/s00202-020-00920-z.

[78] S. Liu, C. Cruzat, and K. Kopsidas, "Impact of transmission line overloads on network reliability and conductor ageing," in *Proc. IEEE Manchester PowerTech*, Jun. 2017, pp. 190–210, doi: 10.1109/PTC.2017.7980857.

[79] R.-A.-M. Dayapera and R. A. Aguirre, "Determination of penetration limit of solar distributed generation (DG) considering multiple bus integration," in *Proc. IEEE PES Asia–Pacific Power Energy Eng. Conf. (APPEEC)*, Oct. 2018, pp. 508–513, doi: 10.1109/APPEEC.2018.8566493.

[80] S. A. Taher and M. H. Karimi, "Optimal reconfiguration and DG allocation in balanced and unbalanced distribution systems," *Ain Shams Eng. J.*, vol. 5, no. 3, pp. 735–749, Sep. 2014, doi: 10.1016/j.asej.2014.03.009.

[81] R. Yan and T. K. Saha, "Voltage variation sensitivity analysis for unbalanced distribution networks due to photovoltaic power fluctuations," *IEEE Trans. Power Syst.*, vol. 27, no. 2, pp. 1078–1089, May 2012.

[82] R. Singh, P. Tripathi, and K. Yatendra, "Impact of solar photovoltaic penetration in distribution network," in *Proc. 3rd Int. Conf. Recent Develop. Control, Autom. Power Eng. (RDCAPE)*, Oct. 2019, pp. 551–556, doi: 10.1109/RDCAPE47089.2019.8979014.

[83] M. M. Haque and P. Wolfs, "A review of high PV penetrations in LV distribution networks: Present status, impacts and mitigation measures," *Renew. Sustain. Energy Rev.*, vol. 62, pp. 1195–1208, Sep. 2016, doi: 10.1016/j.rser.2016.04.025.

[84] M. R. Islam, H. Lu, M. J. Hossain, and L. Li, "Mitigating unbalance using distributed network reconfiguration techniques in distributed power generation grids with services for electric vehicles: A review," *J. Cleaner Prod.*, vol. 239, Dec. 2019, Art. no. 117932, doi: 10.1016/j.jclepro.2019.117932.

[85] T. Simultaneous and M. R. Kaveh, "Simultaneous optimization of re-phasing, reconfiguration and DG placement in distribution networks using BF-SD algorithm," *Appl. Soft Comput. J.*, vol. 4, no. 2, pp. 291–321, 2017, doi: 10.1016/j.asoc.2017.09.041.
[86] F. Shahnia, S. M. Ami, and A. Ghosh, "Circulating the reverse flowing surplus power generated by single-phase DERs among the three phases of the distribution lines," *Int. J. Electr. Power Energy Syst.*, vol. 76, pp. 90–106, Mar. 2016, doi: 10.1016/j.ijepes.2015.09.021.
[87] S. R. Kumar, F. Gafaro, A. Daka, and A. Raturi, "Modelling and analysis of grid integration for high shares of solar PV in small isolated systems—A case of Kiribati," *Renew. Energy*, vol. 108, pp. 589–597, Aug. 2017, doi: 10.1016/j.renene.2017.02.084.
[88] A. Soroudi, A. Rabiee, and A. Keane, "Distribution networks' energy losses versus hosting capacity of wind power in the presence of demand flexibility," *Renew. Energy*, vol. 102, pp. 316–325, Mar. 2017, doi: 10.1016/j.renene.2016.10.051.
[89] M. Usman, F. Bignucolo, R. Turri, and A. Cerretti, "Power losses management in low voltage active distribution networks," in *Proc. 52nd Int. Universities Power Eng. Conf. (UPEC)*, Aug. 2017, pp. 1–6, doi: 10.1109/UPEC.2017.8231882.
[90] Z. Pane, S. Suherman, and R. Sipahutar, "Distributed generators presence impact to the overall system performance," *IOP Conf. Ser., Mater. Sci. Eng.*, vol. 434, no. 1, pp. 329–439, 2014, doi: 10.1088/1757-899X/434/1/012215.
[91] D. Q. Hung, M. R. Shah, and N. Mithulananthan, "Technical challenges, security and risk in grid integration of renewable energy," *Stud. Syst. Decis. Control*, vol. 57, pp. 99–118, Apr. 2016, doi: 10.1007/978-3-319-30427-4_6.
[92] L. M. Cipcigan and P. C. Taylor, "Investigation of the reverse power flow requirements of high penetrations of small-scale embedded generation," *IET Renew. Power Gener.*, vol. 1, no. 3, pp. 160–166, Sep. 2007, doi: 10.1049/iet-rpg:20070011.
[93] A. M. M. Al-Sabounchi, "Optimal sizing and location of photovoltaic generators on three phase radial distribution feeder," Ph.D. thesis, Dept. Technol., Univ. Leicester, Leicester, U.K., 2011. [Online]. Available: https://dora.dmu.ac.uk/bitstream/handle/2086/5225/PhD_Thesis_Ammar%20AL-Sabounchi.pdf?sequence=1
[94] F. R. Segundo Sevilla, V. Knazkins, P. Korba, and F. Kienzle, "Limiting transformer overload on distribution systems with high penetration of PV using energy storage systems," *Int. J. Emerg. Technol. Adv. Eng.*, vol. 6, no. 1, pp. 294–303, 2016. [Online]. Available: https://digitalcollection.zhaw.ch/handle/11475/1826
[95] B. Uçar, T. Istanbul, M. Bärayanék, and G. Kömrgöz, "Influence of PV penetration on distribution transformer aging," *J. Clean Energy Technol.*, vol. 5, no. 2, pp. 131–134, May 2017, doi: 10.18178/jocet.2017.5.2.357.
[96] C. de M. Affonso and M. Kezunovic, "Technical and economic impact of PV-BESS charging station on transformer life: A case study," *IEEE Trans. Smart Grid*, vol. 10, no. 4, pp. 4683–4692, Jul. 2018, doi: 10.1109/TSG.2018.2866938.
[97] L. Novoa, R. Flores, and J. Brouwer, "Optimal renewable generation and battery storage sizing and siting considering local transformer limits," *Appl. Energy*, vol. 256, Dec. 2019, Art. no. 113926, doi: 10.1016/j.apenergy.2019.113926.

ISSAH B. MAJEED (Member, IEEE) received the bachelor's degree in electrical and electronic engineering from the University of Lagos, Nigeria, in 1995, and the M.Sc. degree in electrical and electronic engineering from the University of Mines and Technology, Tarkwa, Ghana, in 2015. He is currently pursuing the Ph.D. degree in electrical and electronic engineering with the University of Johannesburg, South Africa. He is also a part-time Lecturer with the Department of Electrical and Electronic Engineering, Accra Technical University, Ghana. His research interests include the modeling and simulation of power systems, power quality monitoring in distribution systems, and hosting capacity studies for DER grid integration.

NNAMDI I. NWULU (Senior Member, IEEE) is currently a Full Professor with the Department of Electrical and Electronic Engineering Science, University of Johannesburg, and the Director of the Centre for Cyber-Physical Food, Energy and Water Systems (CCP-FEWS). His research interests include the application of digital technologies, mathematical optimization techniques, and machine learning algorithms in food, energy, and water systems. He is a Senior Member of the South African Institute of Electrical Engineers (SMSAIEE). He is a Professional Engineer registered with the Engineering Council of South Africa (ECSA) and a Y-rated Researcher with the National Research Foundation, South Africa. He is the Editor-in-Chief of the *Journal of Digital Food Energy and Water Systems* (JDFEWS) and an Associate Editor of the *IET Renewable Power Generation* (IET-RPG) and the *African Journal of Science, Technology, Innovation, and Development* (AJSTID).